Clinical Cancer Research

Polo-like Kinase 1 Inhibition as a Therapeutic Approach to Selectively Target BRCA1-Deficient Cancer Cells by Synthetic Lethality Induction

Sofía Carbajosa[1], María Florencia Pansa[1], Natalia S. Paviolo[2], Andrés M. Castellaro[3], Diego L. Andino[4], Ayelén D. Nigra[3], Iris Alejandra García[1], Ana C. Racca[3], Lucía Rodriguez-Berdini[3], Virginia Angiolini[1], Laura Guantay[1], Florencia Villafañez[1], María Belén Federico[2], María Celeste Rodríguez-Baili[3], Beatriz L. Caputto[3], Gerard Drewes[5], Kevin P. Madauss[6], Israel Gloger[7], Elmer Fernandez[4], Germán A. Gil[3], José Luis Bocco[1], Vanesa Gottifredi[2], and Gastón Soria[1]

Abstract

Purpose: BRCA1 and BRCA2 deficiencies are widespread drivers of human cancers that await the development of targeted therapies. We aimed to identify novel synthetic lethal relationships with therapeutic potential using BRCA-deficient isogenic backgrounds.

Experimental Design: We developed a phenotypic screening technology to simultaneously search for synthetic lethal (SL) interactions in BRCA1- and BRCA2-deficient contexts. For validation, we developed chimeric spheroids and a dual-tumor xenograft model that allowed the confirmation of SL induction with the concomitant evaluation of undesired cytotoxicity on BRCA-proficient cells. To extend our results using clinical data, we performed retrospective analysis on The Cancer Genome Atlas (TCGA) breast cancer database.

Results: The screening of a kinase inhibitors library revealed that Polo-like kinase 1 (PLK1) inhibition triggers strong SL induction in BRCA1-deficient cells. Mechanistically, we found no connection between the SL induced by PLK1 inhibition and PARP inhibitors. Instead, we uncovered that BRCA1 downregulation and PLK1 inhibition lead to aberrant mitotic phenotypes with altered centrosomal duplication and cytokinesis, which severely reduced the clonogenic potential of these cells. The penetrance of PLK1/BRCA1 SL interaction was validated using several isogenic and nonisogenic cellular models, chimeric spheroids, and mice xenografts. Moreover, bioinformatic analysis revealed high-PLK1 expression in BRCA1-deficient tumors, a phenotype that was consistently recapitulated by inducing BRCA1 deficiency in multiple cell lines as well as in BRCA1-mutant cells.

Conclusions: We uncovered an unforeseen addiction of BRCA1-deficient cancer cells to PLK1 expression, which provides a new means to exploit the therapeutic potential of PLK1 inhibitors in clinical trials, by generating stratification schemes that consider this molecular trait in patient cohorts.

Introduction

BRCA1 and BRCA2 have multiple convergent and divergent functions (1). Initially, it was considered that BRCA1 and BRCA2 had relevance only in hereditary types of breast and ovarian cancers (2, 3). However, a growing set of recent evidence demonstrated that mutations or epigenetic downregulation of *BRCA* genes are also frequently found in sporadic cancers, the acquired deficiency in homologous recombination (HR) being the underlying mechanism of tumorigenesis (4). Moreover, several recent clinical studies have shown that BRCA1/BRCA2–deficient phenotypes are found with high prevalence not only in breast and ovarian cancers, but also in pancreatic, prostatic, and other types of cancers (5).

An iconic successful case to target BRCA-deficient cancers was the development of PARP inhibitors (PARPi). After a decade of intense investigation and substantial investment from companies, three PARPi became available for clinical use: olaparib from AstraZeneca approved in 2015, rucaparib from Clovis approved in 2016, and niraparib from TESARO approved in 2017 (6, 7). Time will be required to weigh the success of PARPi in the clinic. Nonetheless, given the vast incidence of BRCA-deficiencies in

[1]Centro de Investigaciones en Bioquímica Clínica e Inmunología, CIBICI-CONICET, Departamento de Bioquímica Clínica, Facultad de Ciencias Químicas, Universidad Nacional de Córdoba, Córdoba, Argentina. [2]Fundación Instituto Leloir, Buenos Aires, Argentina. [3]Centro de Investigaciones en Química Biológica de Córdoba, CIQUIBIC-CONICET, Facultad de Ciencias Químicas, Universidad Nacional de Córdoba, Córdoba, Argentina. [4]CIDIE-CONICET, Universidad Católica de Córdoba, Córdoba, Argentina. [5]Cellzome AG, Heidelberg, Germany. [6]GlaxoSmithKline-Trust in Science, Global Health R&D, Upper Providence, Pennsylvania. [7]GlaxoSmithKline-Trust in Science, Global Health R&D, Stevenage, United Kingdom.

Note: Supplementary data for this article are available at Clinical Cancer Research Online (http://clincancerres.aacrjournals.org/).

S. Carbajosa and M.F. Pansa contributed equally to this article.

Corresponding Authors: Gastón Soria, Universidad Nacional de Córdoba, Av. Haya de la Torrre s/n, Córdoba, Argentina. Phone/Fax: 54-351-5353850, ext. 55316; E-mail: gsoria@fcq.unc.edu.ar; and Vanesa Gottifredi, IIBBA, Fundacion Instituto Leloir, CONICET, Av. Patricias Argentinas 435, C1405 BWE, Buenos Aires, Argentina. E-mail: VGottifredi@leloir.org.ar

Clin Cancer Res 2019;25:4049–62

doi: 10.1158/1078-0432.CCR-18-3516

Translational Relevance

In this work, we unveiled a strong synthetic lethal interaction between the mitotic kinase PLK1 and the tumor suppressor BRCA1. We confirmed the selective cytotoxicity of PLK1 inhibition by developing *in vitro* and *in vivo* models that emulate the coexistence of healthy BRCA1-proficient cells and BRCA1-deficient cancer cells found in patients. These results were extended by the clinical finding that tumors with low-BRCA1 expression, which are mostly basal like and triple negative for hormone receptors, depict the highest levels of PLK1 expression. Given that PLK1 inhibitors are currently being studied in late-stage clinical trials, these preclinical and clinical discoveries stimulate the design of clinical studies considering the BRCA1 status of patients as a marker of therapeutic response.

human cancers, there is a major need to develop new targeted therapies that exploit such deficiencies from different angles. This is also particularly relevant given that many types of resistance mechanisms to PARPi are already being described (8).

In a cancer therapy context, synthetic lethality (SL) can be defined as the selective toxicity triggered by a given treatment on a cancerous cell with a given genetic defect in comparison with the healthy cells of the patient. Despite its great potential (9), SL remains largely unexploited in cancer drug discovery. This could be attributed, at least in part, to the lack of suitable screening technologies that comprehensively cover critical variables for SL induction, such as: (i) sufficient experiment length for SL to manifest; (ii) isogenicity between the cell lines compared, to unequivocally attribute the SL induction to a given genetic defect; (iii) broad coverage of the cell lines heterogeneity, to avoid misleading conclusions due to clonal events; (iv) high sensitivity and comparability, to unveil small differences in cell survival between the cell lines compared in the screening. Most of the survival assays currently used for cancer drug discovery are based on metabolic readouts such as ATP levels. Because these methods involve measuring technologies with great throughput capacity, they have become the gold standard for high-throughput screenings. However, such technologies have several biology-related setbacks that make them unsuitable for SL-based screenings. For instance, metabolic readouts show poor correlation with the absolute number of cells and become less sensitive when cells reach high confluence in long-term assays (10–12). Moreover, these methods do not provide information at single-cell level. Thus, all comparisons must be performed between different wells/plates, with a substantial increase in variability and loss of comparability and sensitivity.

In this article, by combining fluorescent tagging, lentiviral transduction of shRNAs against BRCA1 and BRCA2 and high-throughput flow cytometry, we developed an SL-based phenotypic screening assay, which tackles all the critical points mentioned above. Then, we used our assay to screen the second generation of a public library of 680 kinase inhibitors (PKIS2). We found that the inhibition of Polo-like kinase 1 (PLK1) triggers strong SL in BRCA1-deficient cancer cells. Because PLK1 is a central kinase for mitotic progression that is currently under clinical investigation (13), our results put forward valuable evidence for positioning PLK1 inhibitors in patients' groups characterized by alterations in BRCA1 expression.

Materials and Methods

DNA constructs and shRNA

iRFP-C1 was a gift from Michael Davidson and Vladislav Verkhusha (National Magnetic High Field Laboratory, Tallahassee, FL; Addgene plasmid #54786; ref. 14); shBRCA1 (TRCN0000010305, Sigma-Aldrich) was cloned into pLKO.1-TRC vector through EcoRI and AgeI restriction sites; and shSCR-pLKO.1 was described previously (15). shSCR-plenti (TR30021) and shPLK1-plenti (TL320457 A) were acquired from Origene. pDRGFP and pCBASceI were a gift from Maria Jasin (Memorial Sloan Kettering Cancer Center, New York, NY; ref. 16).

Antibodies

Primary antibodies used were as follows: α-BRCA1 (Oncogene Research-Ab1); KU70 (#ab3114); α-PLK1 (#4513S); α-Tubulin (#T9026); γ-tubulin (Sigma-Aldrich); phalloidin-Alexa Fluor 488 (Molecular Probes); α γH2AX Ser 139, Upstate (Millipore, clone JBW301); α 53BP1 (#SC-22760), α-pPLK1^{T210} (#9111). Secondary antibodies used were goat α-mouse IRDye 680RD and goat α-rabbit IRDye 800CW from LI-COR Biosciences; α-mouse/rabbit–conjugated Cy2/Cy3 antibodies (Jackson ImmunoResearch). Nuclei were stained with DAPI (Sigma).

Cell lines and cell culture

HCT116$^{p21-/-}$ cells were kindly provided by Bert Vogelstein (Johns Hopkins Medicine, Baltimore, MD). V-C8 cell lines were supplied by Bernard Lopez (Institut Gustave Roussy, Villejuif, France). All the remaining cells used in this study were obtained from ATCC. Cell culture was performed in DMEM medium (Thermo Fisher Scientific) supplemented with 10% FBS (GIBCO-NZ) and 1% penicillin/streptomycin. Control for *Mycoplasma* contamination was performed periodically with a PCR-based method with internal loading control. Cell lines were used for experimentation for no more than 20 passages from the main frozen stock.

Generation of fluorescent-tagged stable cell lines

Transfection protocols were performed using JetPrime (Polyplus-transfection) according to the manufacturer's instructions. Multiple rounds of cell sorting (3–5) were performed (FACS Aria II, BD Bioscience). The lentiviral titer was determined by serial dilution and transduction of HCT116 stably expressing iRFP cells followed by scanning using Odyssey CLX System (LI-COR Biosciences). The minimum lentiviral titer that promoted maximum survival of the transduced cells after puromycin selection was determined. From the point of maximum survival after puromycin addition, increasing lentiviral titers were used. The points that show the higher down-regulation BRCA1 and BRCA2 by qPCR and Western blotting, yet keeping similar proliferation rates to the shSCR-transduced cell lines, were selected for the screening. The entire screening phase was performed with cells that did not exceed 5 passages after transduction to avoid the positive selection of cells with higher BRCA levels.

Protein analysis

For direct Western blot analysis, samples were lysed in commercial Laemmli Buffer (Bio-Rad) with reducing agent 2-mercaptoethanol. The detection and quantification were performed with Odyssey CLX System (LI-COR Biosciences) using the proprietary Image Studio Software.

qRT-PCR

tRNA was isolated using TRIzol reagent. Reverse transcription was performed and BRCA2 mRNA levels were measured with forward,-5′-AGGGCCACTTTCAAGAGACA3′ and reverse,5′TAG-TTGGGGTGGACCACTTG3′ primers using the iQ SYBR Green Supermix (Invitrogen). Relative expression levels were normalized to GAPDH.

HR analysis

We used an HR assay generated previously in U2OS cells containing an integrated HR reporter substrate DR-GFP (16) with some modifications described previously (17).

Cell-cycle analysis and apoptosis assay

For cell cycle, cells were prepared as described previously (17). Stained samples were subjected to FACS and data were analyzed using FlowJo Software (FlowJo LLC). Cell apoptosis was detected using the Annexin V Apoptosis Detection Kit (sc-4252 AK, Santa Cruz Biotechnology).

Immunostaining and microscopy

Cells were fixed in 2% (w/v) paraformaldehyde (PFA)/2% sucrose and permeabilized with 0.1% (v/v) Triton X-100 in PBS. Blocking during 2 hours at room temperature in PBS 2% (v/v) donkey serum (Sigma) was performed. Coverslips were incubated for 1 hour in primary antibodies and then 1 hour in secondary antibodies. Images were obtained with an inverted fluorescence microscope (LEICA DMI8).

Chromosomal aberration analysis

Metaphase chromosome spreads were performed according to described protocols (18). Samples were analyzed in an Applied Imaging Cytovision 3.7. 50 metaphase spreads were used to quantify chromosomal gaps, breaks, and exchanges.

Micronucleus assay

Cells seeded at low density were treated. After 24 hours, cells were incubated with cytochalasin B (4.5 μg/mL, Sigma), and micronucleus (MN) determination was performed as described previously (19).

Clonogenic assays

Cells were plated in 24-well plates at seeding density of 2×10^4 cells per well and then treated for 6 days. The remaining cells were trypsinized, counted, and seeded at extremely low density in 24-well plates. After 10 days of culture, the media was removed, and crystal violet staining solution was added for colony visualization. The surviving fraction was determined as described in (20).

Generation of chimeric spheroids

The spheres were formed from an equimolar mixture of cells (750 of each cell line) using the hanging drop system of Perfecta3D 96-well plates (3D Biomatrix). The partial medium exchange was made every alternate day. After treatment, the spheres were harvested via air displacement and incubated with 0.25% trypsin for 5 minutes and disintegrated mechanically. After the washing step, the cells were acquired in FACSCanto II (BD Bioscience).

Double tumor xenograft model

A total of 1.5×10^6 cells were injected into each flanks of 6- to 8-week-old nude mice using a G27 syringe. When tumors reached approximately 50 to 100 mm^3, animals were randomized into treatment and control groups of 5 mice each. Volasertib was diluted in ethanol, resuspended in 0.5% natrosol 250 hydroxyethyl-cellulose, and administered intragastrally via gavage needle. The animals were weighed, and tumor volumes were determined thrice a week using an Electronic Caliper (Mitutoyo). The results were converted to tumor volume (mm^3) by the formula length $\times$ width2 $\times$ $\pi/6$. Ulcerations that appeared in the fast-growing control tumors after day 14 were treated daily using povidone–iodine. At day 21 (tumor volume $\sim$ 1,000 mm^3), mice were euthanized. Protocol approved by CICUAL-UNC.

MDA-436 double tumor xenograft model

A modified protocol from (21) was used. Briefly, 5×10^6 MDA-436 cells in a final volume of 100 μL of 50% complete media + 50% Matrigel were xenografted into each of the fourth mammary gland of 6- to 8-week-old nude mice using a G27 syringe. When tumors reached an average size between approximately 50 to 100 mm^3, animals were randomized into treatment and control groups. Protocol approved by CICUAL-UNC.

Statistical analysis

Graphs and statistical analysis were performed using GraphPad Prism 5.0 (GraphPad Software), applying the Student *t* test and ANOVA test as appropriate.

Results

Development of a survival screening method to identify SL interactions in BRCA1- and BRCA2-deficient backgrounds

To identify novel SL interactions in BRCA-deficient contexts, we developed a phenotypic screening pipeline using high-throughput flow cytometry. We generated stable cell lines tagged with fluorescent proteins that express shRNAs against BRCA1 and BRCA2 (Fig. 1A). The knockdown approach using lentiviral shRNA allowed us to work with transduced cellular pools that avoid the bias of clonal selection yet keeping isogenicity. The BRCA1 and BRCA2-deficient cell lines used in the screening were generated by selecting a lentiviral transduction titer that caused substantial knockdown, but without affecting the proliferation proficiency (Fig. 1B). This is a critical issue, because a hallmark of our screening platform is that BRCA-deficient and BRCA-proficient cells are cocultured in the same well. As such, each well behaves as a single screening unit with an internal control (shSCR), allowing the assessment of SL in both BRCA-deficient populations simultaneously (Fig. 1A). The three cell lines are cocultured together for 6 days in the presence of the tested compounds (Fig. 1C, left). The final readout is the total cell number of each cell population, which is determined by acquiring the complete well using an acoustic flow cytometer. Three types of outcomes are possible for every tested compound: (i) nontoxic, (ii) toxic but not selective, and (iii) SL (Fig. 1C, right). To calibrate the sensitivity of the platform we performed dose–response experiments using the PARPi olaparib (Fig. 1D). In addition, to promote the identification of compounds, we added an ultra-low dose of camptothecin as a sensitizer in the culture media (0.1 nmol/L CPT). We confirmed that while such a low amount of CPT did not impair the survival of BRCA-proficient and BRCA-deficient populations,

it promoted SL induction at doses of olaparib that do not induce SL as a mono drug (Supplementary Fig. S1A).

After evaluating various cell lines, we selected HCT116$^{p21-/-}$ cells as the optimal parental cell line for this platform. Two main factors were considered for this choice. First, this cell line proved to be amenable for culture from high dilution factors and for several days, reaching uniform confluence in a 96-well format. Second, this cell line showed the strongest SL response to olaparib when BRCA1 or BRCA2 was downregulated by lentiviral shRNA (Fig. 1D; Supplementary Fig. S1B). Because the lack of p21

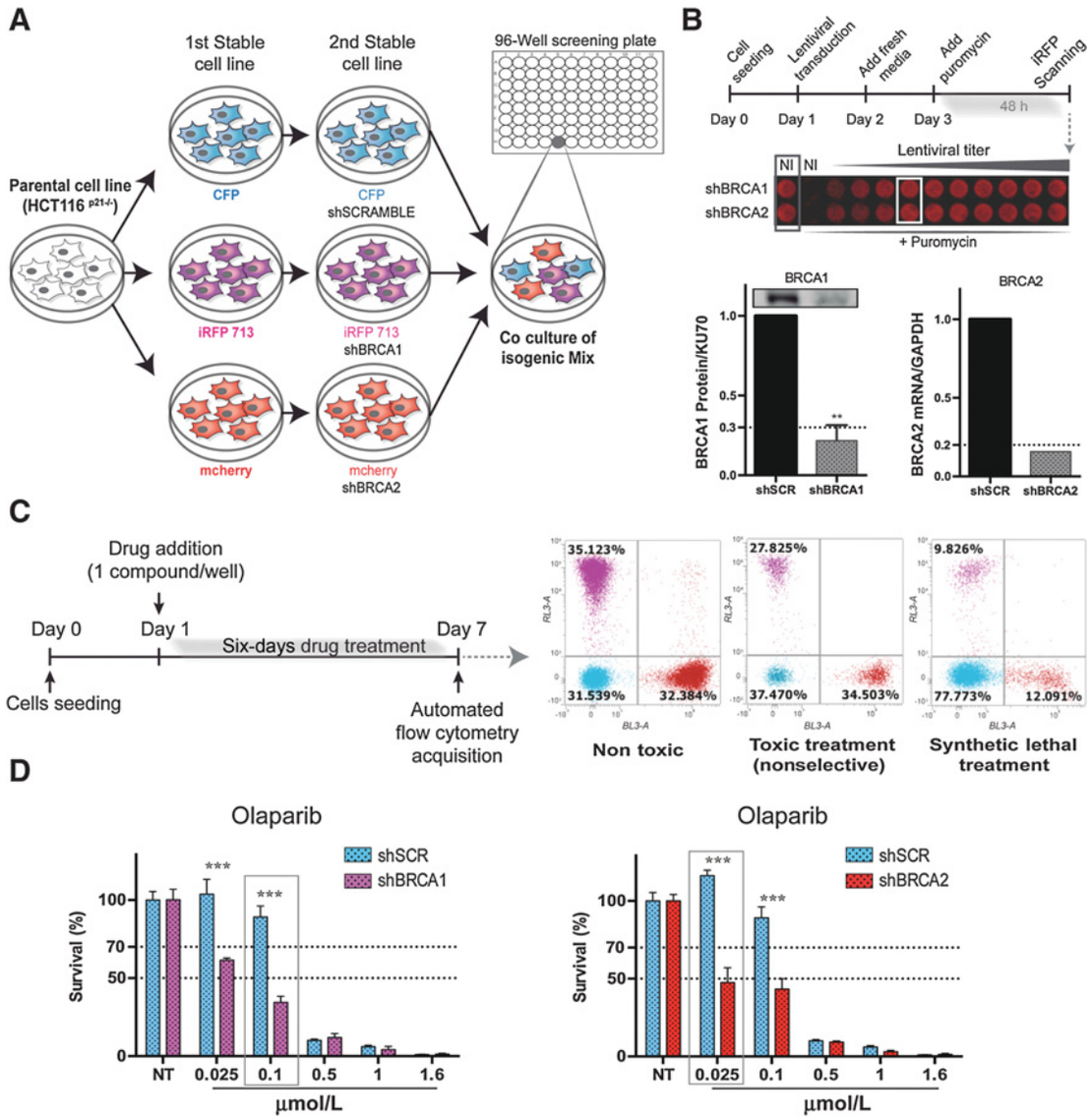

Figure 1.

Phenotypic screening platform to simultaneously search for SL interactions with BRCA1 and/or BRCA2. **A,** Layout of the generation of the double stable cell lines tagged with different fluorescent proteins (CFP, iRFP, and mCherry) and expressing shRNAs for BRCA1 or BRCA2. The screening assay consists in the coculture of these isogeneic BRCA-proficient and BRCA-deficient cell lines in equal proportions using a 96-well plate format. **B,** Protocol used to titrate the shRNA lentiviral preparations. Serial dilutions of the supernatant containing the lentivirus were used to transduce HCT116$^{p21-/-}$ cells stably expressing iRFP (the white square highlights the puromycin dose of maximum survival from which the stable cell lines are generated). The downregulation reached for BRCA1 and BRCA2 is shown by Western blot and qPCR, respectively. **C,** Timeline of the screening protocol and the three types of responses observed for the tested compounds: nontoxic (the absolute number of cells and the ratio between the populations' percentage remains unchanged); not selective toxicity (the absolute number of cells from each population decreases, but the ratio remains unchanged); and SL (the ratio between populations' percentage is altered, with selective toxicity in the BRCA1- and/or BRCA2-deficient populations). **D,** Calibration of the screening platform with a dose–response curve of the PARPi olaparib, which was used as positive control of SL induction in the screening plates. The gray squares highlight the optimal SL doses of olaparib, which induce the maximum survival difference between the shBRCA and the shSCR cell lines. Data plotted as mean and SD of three independent experiments. Statistical analysis was performed using two-way ANOVA with Bonferroni posttest (***, $P \leq 0.001$).

attenuates G_1/G_2 checkpoints (22), these cells are prone to enter an apoptotic program, avoiding the prolonged p21-dependent cell-cycle arrest that could mask an SL condition in the time frame of the experiment. For screening purposes, hits were defined by a variation greater than 5 SDs on two survival-related values: (i) fold of SL induction: calculated from the ratios of the different populations within the same well and (ii) survival difference: calculated from the differential survival when comparing a given treatment to the untreated wells from the same plate. A detailed example illustrating the calculation and implications of these values is shown in Supplementary Fig. S1D.

SL screen targeting the human kinome

With the aim of discovering novel druggable pathways to treat BRCA-deficient cancers, we screened a library of kinase inhibitors provided by GlaxoSmithKline (PKIS2: The Public Kinase Inhibitor Set #2). This library comprises 680 ATP-competitive inhibitors with a broad coverage of the human kinome (23, 24). To minimize the pleiotropic effect of ATP-competitive inhibitors (25), we performed the screening at a low dose (0.1 μmol/L). Strikingly, we found that 10 PLK1 inhibitors (PLKi) induced potent SL in the BRCA1-deficient population (Fig. 2A; Supplementary Table S1). Remarkably, one PLK1i (GSK978744A) induced even a higher fold of SL induction and survival difference than the optimal dose of olaparib, highlighting its high selectivity and low unspecific toxicity at this dose (Fig. 2A). Early validation experiments using the 10 hits plus other PLK1i available in the PKIS2 library allowed us to rank the Top 6 PLKi by their optimal doses of SL induction (Fig. 2B). Three of them (GSK978744A, GSK483724A, and GSK580432A) showed an SL induction capacity similar to the optimal dose of olaparib (Fig. 2B) and were therefore selected for validation experiments. Noteworthy, at higher doses of each inhibitor the SL induction range is lost due to the increase in unspecific toxicity (Fig. 2C), as we also observed for olaparib (Fig. 1D). Moreover, the sensitization with CPT was not necessary for SL induction, thus demonstrating that PLK1 inhibition alone suffices to induce SL in BRCA1-deficient backgrounds (Fig. 2D).

Validation of PLK1 inhibition as an SL trigger in BRCA1-deficient cellular models

To discard the possibility that the SL induction could be related to the coculture conditions of shSCR and shBRCA1 cells, we performed SL induction experiments in which each isogenic cell line was cultured in separate wells (Fig. 2E). As a second pharmacologic approach we used a PLK1 inhibitor from Boehringer Ingelheim (BI-6727: volasertib), which is currently in phase III clinical trials (26). Using this drug in the nanomolar range, we confirmed the results obtained using the PLK1 inhibitors from GSK. Volasertib SL-inducing activity peaked at 6 days posttreatment in a dose range between 5 and 10 nmol/L, where cytotoxicity was found almost exclusively in the BRCA1-deficient population (Fig. 2F and G).

We next validated volasertib in multiple breast cancer backgrounds. Using lentiviral vectors expressing shRNAs for BRCA1, we first transduced T47D cells (Fig. 2H). We also compared nonisogenic BRCA1-KO (MDA-436) versus BRCA1-WT (MDA-231) cell lines (27) and isogenic HCC1937 BRCA1-KO versus its complemented counterpart (Fig. 2H). We found that PLK1 inhibition was more toxic in all the BRCA1-deficient backgrounds, in particular, in KO cells (Fig. 2H). Remarkably, SL induction after volasertib treatment was also observed in other type of cancer cells such as ovarian cancer cells and osteosarcoma cells, and even in nontumoral mouse embryonic fibroblasts expressing shRNAs for BRCA1 (Supplementary Fig. S2A). An additional line of evidence was obtained using a genetic approach in which instead of inhibiting PLK1, we downregulated PLK1 expression using lentiviral shRNAs. With this method, we also observed induction of SL in BRCA1-deficient cells (Fig. 2I).

Importantly, most of the experiments previously described to investigate the SL interaction between BRCA1 and PLK1 were also performed using isogenic BRCA2-deficient backgrounds (Supplementary Fig. S2B–S2F). From these experiments we concluded that while PLK1 inhibition triggers mild SL in BRCA2-deficient cells, this effect is much more robust in BRCA1-deficient cells. Using the direct repeats assays (DR-GFP) from Maria Jasin's Lab, we concluded that the knockdown of BRCA1 and BRCA2 led to the impairment of HR (Supplementary Fig. S2G), which is in line with their similar SL response to olaparib (Fig. 1D). Moreover, we also observed that volasertib treatment within the dose range that triggers SL does not impair HR efficiency (Supplementary Fig. S2H). Taken together, these data suggest that the HR impairment induced by the downregulation of BRCA1 and BRCA2 is not the SL trigger associated to PLK1 inhibition, but more likely an independent function of BRCA1. Therefore, we focused the following experiments in BRCA1-deficient models.

BRCA1 downregulation leads to aberrant transition through M-phase after PLK1 inhibition

Because of its central role in regulating several factors that promote mitotic progression, PLK1 inhibition causes a robust arrest in M-phase (28). Thus, we decided to evaluate whether the observed SL was associated to alterations in the robustness of the M-phase arrest in BRCA1-proficient versus BRCA1-deficient cells. We hypothesized that PLK1 inhibition could trigger a stronger G_2–M arrest in BRCA1-deficient cells, which could, in turn, trigger SL. However, our results revealed a different scenario. Cell-cycle analysis by flow cytometry at 6 days posttreatment showed that the accumulation of BRCA1-deficient cells in G_2–M was similar, or even attenuated, within the dose range of volasertib that triggers SL induction (Fig. 3A; Supplementary Fig. S3A). However, the slow recovery of BRCA-deficient cells from the G_2–M arrest correlated with a concomitant increase in the sub-G1 population (Fig. 3A; Supplementary Fig. S3A) and with the induction of apoptosis/necrosis, which was evaluated using Annexin V/propidium iodide (PI) staining (Fig. 3B). Given that both shSCR and shBRCA1 cells grow at equivalent rates (Fig. 1C), these results suggest that the deficiency in BRCA1 expression generates a disadvantage to transition across M-phase in the context of PLK inhibition. Interestingly, experiments using the well-characterized mitotic poisons nocodazole and colcemide showed that these drugs also induced SL in BRCA1-deficient cells (Fig. 3C), hence reinforcing the notion that BRCA1-depleted cells display an impaired ability to recover from M-phase arrest. However, these drugs induced a much weaker SL response in comparison with the one triggered by PLK1 inhibitors. Thus, we concluded that the SL induction triggered by PLK1 inhibition could not be attributed simply to the strength of the G_2–M-phase arrest, but more likely to an altered G_2–M transition.

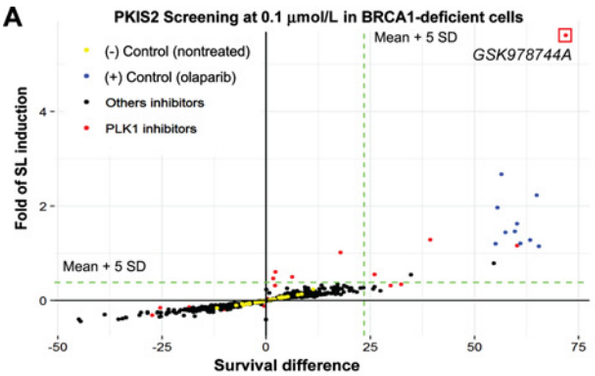

B

Top hits in BRCA1-deficient cells

PLK1 inhibitors	Optimal concentration [nmol/L]	Surv Diff (%)
GSK978744A	150	**75.9**
GSK483724A	100	**57.9**
GSK580432A	25	**46.2**
GSK326090A	100	**39.4**
GSK237700A	500	**30.8**
GW852849X	100	**26.0**
Olaparib	100	**54.7**

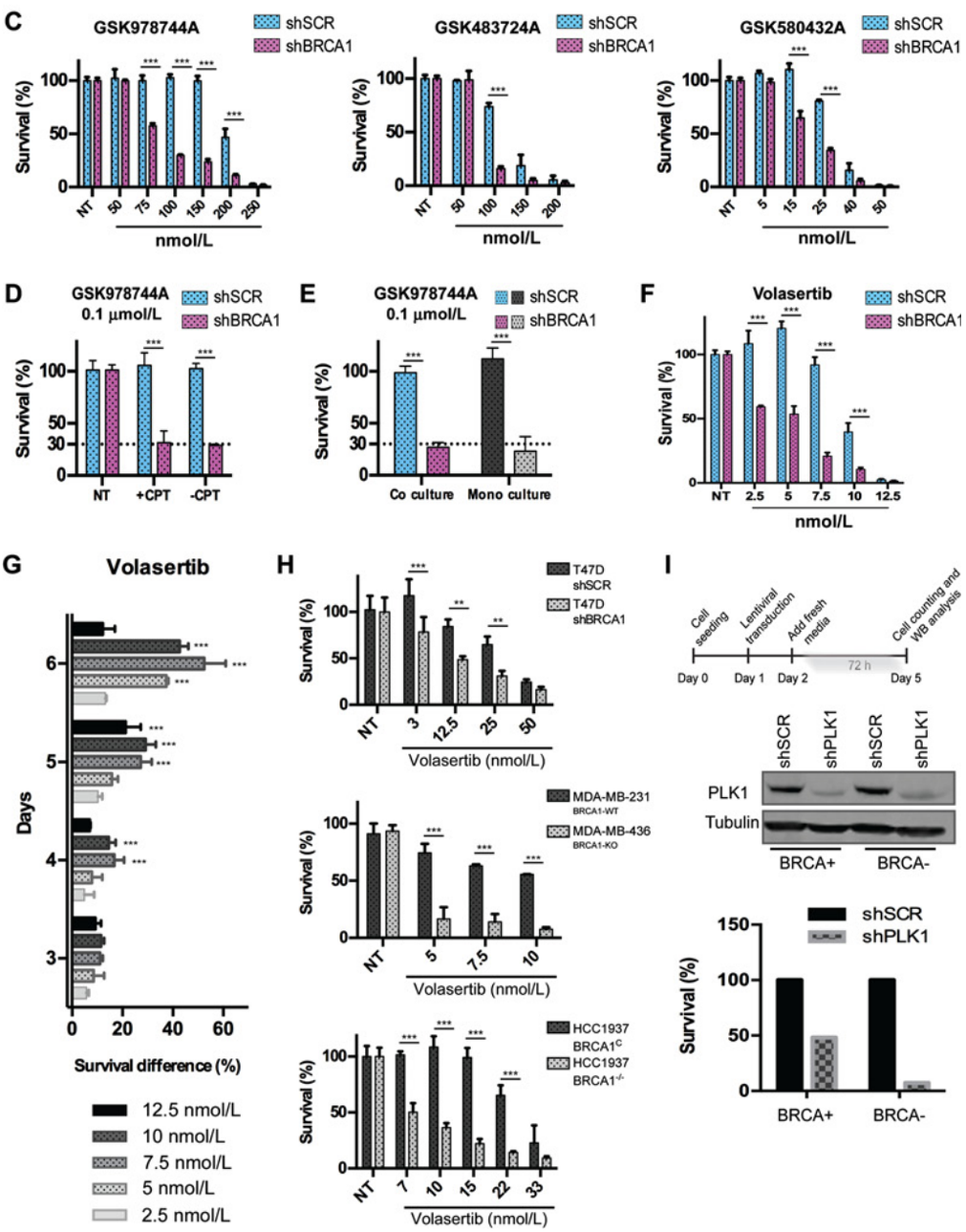

To evaluate which mitotic progression features could be differentially altered in BRCA1-deficient cells, we investigated previous reported roles for BRCA1 in mitotic progression. We found several reports indicating that BRCA1 is involved in centrosomal duplication (29–37). Because PLK1 has complementary roles in this process (38), we decided to evaluate the centrosomal number and distribution in PLK1-inhibited cells. Strikingly, we found that PLK1 inhibition leads to the accumulation of giant multinucleated cells with large aggregates of centrosomes that systematically locate in the cellular center (Fig. 3D; Supplementary Fig. S3B). These results indicate that PLK1 inhibition causes aberrant mitosis, promoting the finalization of karyokinesis without the completion of cytokinesis.

A hypothesis that derived from the additive contribution observed between BRCA1 knockdown and PLK1 inhibition in mitotic progression was that the surviving multinucleated cells should present a low remnant proliferative capacity. Thus, we performed clonogenic experiments by replating the cells that survive to 6 days of treatment with volasertib or olaparib (Fig. 3E). As expected, we observed that BRCA1-deficient cells treated with volasertib displayed a lower clonogenic potential than BRCA1-proficient cells, a similar result to that observed for olaparib (Fig. 3E).

SL induction by PLK1 inhibition is not associated with acute replication stress and genomic instability

Our previous results suggested that PLK1 could be positioned as an alternative to PARP inhibition to selectively target BRCA1-deficient cells. Thus, we decided to evaluate whether PLK1 inhibition also increases genomic instability of BRCA1-deficient cells, as it is well known for PARPi (39, 40). Initially, we evaluated two widely used markers of DNA damage, namely γH2AX and 53BP1 foci formation. As a positive control, we used olaparib. Surprisingly, volasertib did not induce foci formation even at the higher doses where it triggers SL induction (Fig. 4A; Supplementary Fig. S4). Thus, we thought that volasertib might not activate an acute DNA damage response but could induce lower levels of DNA damage, which require a more sensitive readout. Therefore, we decided to perform cytogenetic analyses to search for chromosomal aberrations associated with the generation of single- and double-strand breaks, namely chromosomal gaps/breaks and exchanges. We observed that while olaparib treatment substantially increased the number of breaks and exchanges/metaphase, volasertib did not increase the basal proportion of any type of chromosomic aberrations (Fig. 4B). A similar result was obtained using a micronuclei assay, where the number of micronuclei increased after olaparib treatment, but not after volasertib (Fig. 4C). Together, these results indicate that the mechanism of SL induction triggered by PLK1 inhibition is different to the one of olaparib, which might position volasertib as a therapeutic alternative to target BRCA-deficient cancers.

PLK1 triggers SL in a model of BRCA1^{+}/BRCA1^{-} chimeric spheroids

To investigate deeper into the therapeutic potential of PLK1 inhibition in BRCA-deficient cancers, we developed a three dimensional (3D) cell culture model. We generated chimeric spheroids by mixing equal amounts of BRCA1-proficient and -deficient cells tagged with fluorescent proteins. Established spheroids were treated with volasertib for 6 days and then mechanically disaggregated and analyzed by flow cytometry (Fig. 5A), using the same survival parameters selected for the screening pipeline (Supplementary Fig. S1D). Unexpectedly, a marked increase in the proportion of BRCA1-deficient cells was observed in the untreated spheroids, thus suggesting that BRCA1 deficiency provides a proliferative advantage in this type of 3D models (Supplementary Fig. S5A). Nonetheless, the analysis of the relative survival allowed us to conclude that the treatment with olaparib and volasertib induces a comparable SL response in BRCA1-deficient cells (Fig. 5B). Olaparib-treated spheroids were similar in size than spheroids treated with high doses of volasertib, but the latter were less compact and more prone for disruption of the outer layers (Fig. 5C; Supplementary Fig. S5C). We also observed that spheroids were much more resistant to higher doses of volasertib than cell monolayers, depicting a clear dose–response behavior when analyzing the internal percentages of both cell populations in each pool of spheroids as independent experimental units (Supplementary Fig. S5B).

Development of an animal model to study SL induction *in vivo*

The data obtained using *in vitro* models prompted us to investigate whether the SL induction also takes place *in vivo*. The complexity to address this issue relies on the fact that PLK1 inhibition *per se* has an antitumoral effect (13), showing strong cytotoxic activity independently of the BRCA1 status (see higher

Figure 2.

PLK1 inhibition is SL with BRCA1 deficiency. **A,** Screening results with the PKIS2 library from GlaxoSmithKline. The graph shows the fold of SL induction and the survival difference after the treatment with 680 kinase inhibitors in the BRCA1-deficient population. Olaparib 100 nmol/L was used as positive control in each screening plate. Ten PLK1 inhibitors were identified as hits using the criteria of more than 5 SDs in any of the variables. The most potent PLK1 inhibitor, GSK978744A, is highlighted within a red square. Z prime analysis was performed as $Z' = 1 - 3(\sigma p + \sigma n)/|\mu p - \mu n|$, where "p" is olaparib survival difference and "n" is the survival difference of the nontreated samples. **B,** Early dose–response validation with all the PLK1 inhibitors available in the library. The table shows the top 6 inhibitors and the optimal dose at which they induce the highest survival difference (Surv Diff) between isogenic BRCA1-proficient and BRCA1-deficient cells. Olaparib is depicted for comparative purposes. **C,** Full dose–response experiments with the top 3 PLK1 inhibitors in HCT116$^{p21-/-}$ cells, showing the survival of the isogenic shBRCA and shSCR cell lines. **D,** SL induction with GSK978744A in BRCA1-deficient cells with or without the addition of 0.1 nmol/L CPT as a sensitizer. **E,** SL induction with GSK978744A using shSCR and shBRCA1 cells in coculture, as in the screening assay, or as monoculture in parallel wells. **F,** Dose response SL induction with a commercial PLK1 inhibitor, volasertib (BI-6727), in coculture of HCT116$^{p21-/-}$. **G,** Dose response using volasertib in a time course monoculture experiment from 3 to 6 day endpoints, showing the survival difference between shBRCA1 and shSCR cells. **H,** Validation of the SL response to volasertib using three pairs of breast cancer cell lines in monoculture experiments: T47D^{shSCR} versus T47D^{shBRCA1}, MDA-231$^{BRCA1\text{-}WT}$ versus MDA-436$^{BRCA1\text{-}KO}$, and HCC1937$^{BRCA1\text{-}KO}$ versus HCC1937$^{BRCA1\text{-}C}$. **I,** Protocol of shRNA-mediated knockdown of PLK1 in HCT116$^{p21-/-}$ cells. The Western blot (WB) on the central panel shows equivalent levels of PLK1 knockdown reached in shSCR and shBRCA1 cells. Bottom, decreased survival observed in BRCA-deficient cells after the downregulation of PLK1. Survival was calculated by the total cell count in each well after PLK1 knockdown for 72 hours. Statistical analysis was performed using two-way ANOVA with Bonferroni posttest (***, $P \leq 0.001$; **, $P \leq 0.01$).

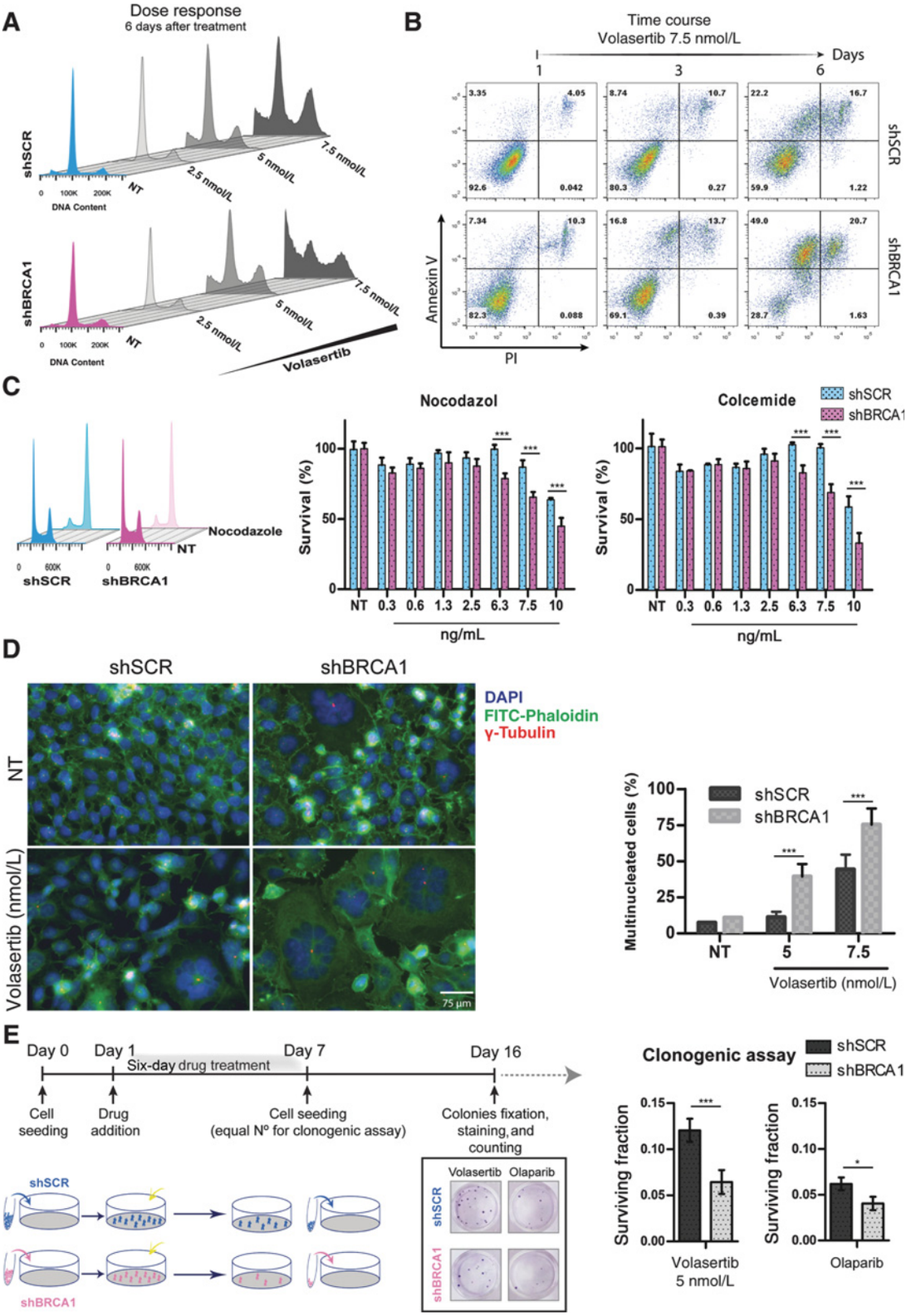

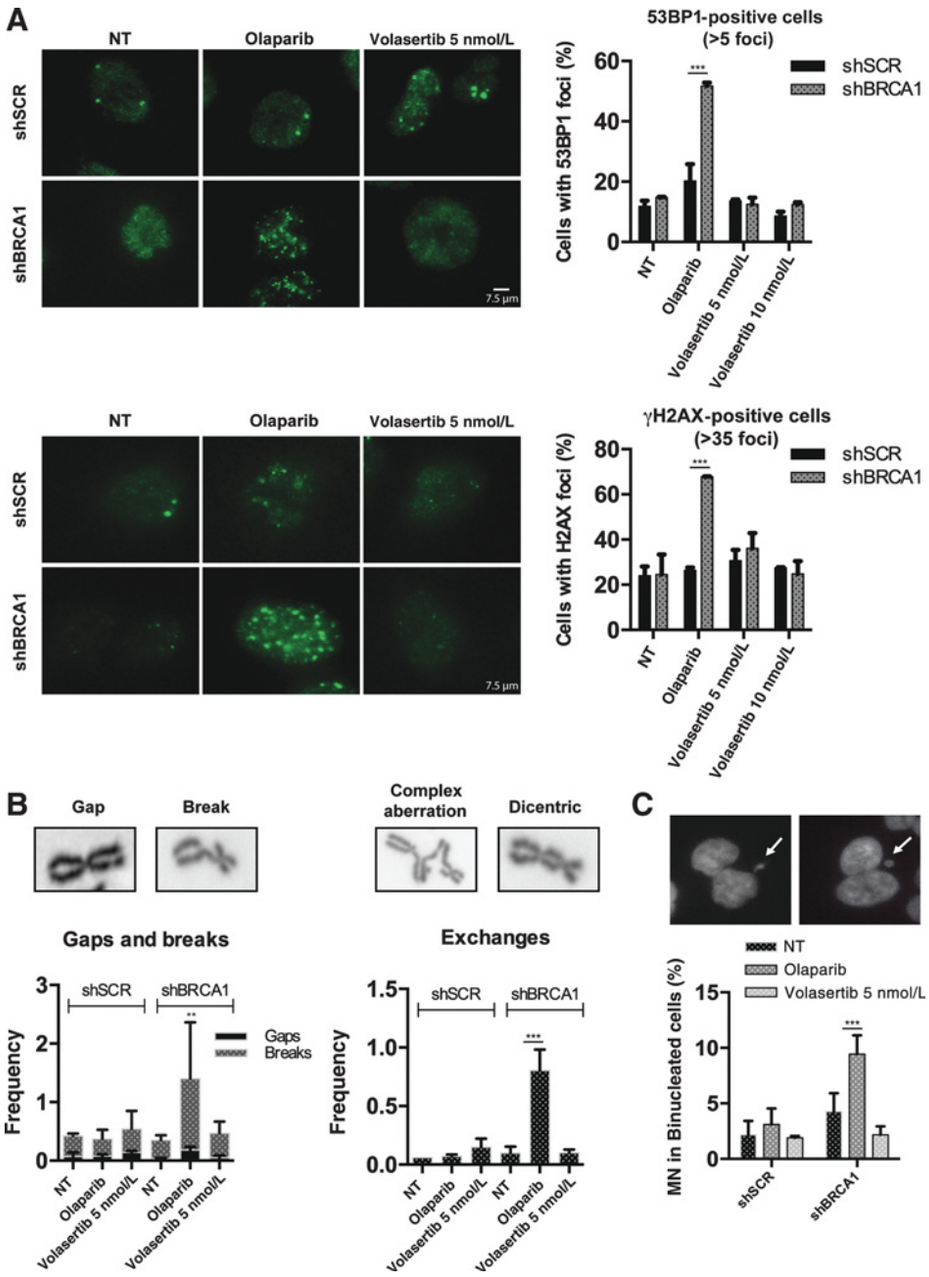

Figure 4.
Volasertib does not induce DNA damage or chromosomic aberrations at SL doses. **A,** HCT116$^{p21-/-}$ shSCR and shBRCA1 cells were treated with volasertib or olaparib. Forty-eight hours later, immunostaining with 53BP1 and γH2AX antibodies was performed. The percentage of cells with foci for these two DNA damage markers was quantified using fluorescence microscopy (magnification: 100×). Only nuclei with more than 5 foci of 53BP1 were quantified as positive. Cells with more than 35 γH2AX focal structures were considered positive. At least 300 cells per condition were analyzed. Statistical analysis was performed using two-way ANOVA with Bonferroni posttest (***, $P \leq 0.001$). **B,** HCT116$^{p21-/-}$ BRCA1-proficient and -deficient cells were submitted for cytogenetic analysis 48 hours after the treatment with volasertib or olaparib. The frequency of gaps, breaks, and exchanges was calculated after analyzing a minimum of 70 metaphases per condition. **C,** HCT116$^{p21-/-}$ BRCA1-proficient and -deficient cells were treated for 24 hours using volasertib or olaparib and were arrested at a binucleated stage using cytochalasin B. The frequency of micronuclei was estimated using DAPI staining and fluorescence microscopy (magnification: 100×), analyzing a minimum of 300 binucleated cells per condition. Two-tailed unpaired *t* test was used (***, $P \leq 0.001$; **: $P \leq 0.01$).

Figure 3.
The combination of PLK1 inhibition and BRCA1 deficiency triggers aberrant mitotic transition and leads to decreased clonogenic potential. **A,** DNA content profiles using propidium iodide (PI) to compare the cell-cycle progression of HCT116$^{p21-/-}$ shSCR and shBRCA1 cells treated with volasertib. **B,** Quantification of apoptosis/necrosis induction of HCT116$^{p21-/-}$ shSCR and shBRCA1 cells stained with Annexin V-FITC and PI after treatment with the optimal SL dose of volasertib (7.5 nmol/L). **C,** Dose–response experiment that shows the SL induction triggered by the mitotic poisons nocodazole and colcemide in BRCA1-deficient cells. Left, control of the M-phase arrest triggered by 10 ng/mL nocodazole. Statistical analysis was performed using two-way ANOVA with Bonferroni posttest (***, $P \leq 0.001$). **D,** shSCR and shBRCA1 HCT116$^{p21-/-}$ cells were treated with DMSO or volasertib. Six days later, immunofluorescences were performed using γ-tubulin (red) to stain the centrosomes, phalloidin (green) to delimitate the cytoplasm, and DAPI to stain the nuclei. Images were taken with an inverted fluorescence microscope (magnification: 60×). Right, the quantification of cells with more than 3 nuclei (or two nuclei with a single centrosome) for each condition is shown at both 5 and 7.5 nmol/L of volasertib. At least 1,000 cells per condition were analyzed. Statistical analysis was performed using two-way ANOVA with Bonferroni posttest (***, $P \leq 0.001$). **E,** Left, summary of the protocol used to evaluate the clonogenic potential of the surviving population to volasertib treatment in HCT116$^{p21-/-}$ shSCR and shBRCA1 cells. An example of 1 plate for each condition stained with crystal violet is depicted. Right, the quantification of the surviving fraction of three independent experiments. Two-tailed unpaired *t* test (***, $P \leq 0.001$; *, $P \leq 0.05$).

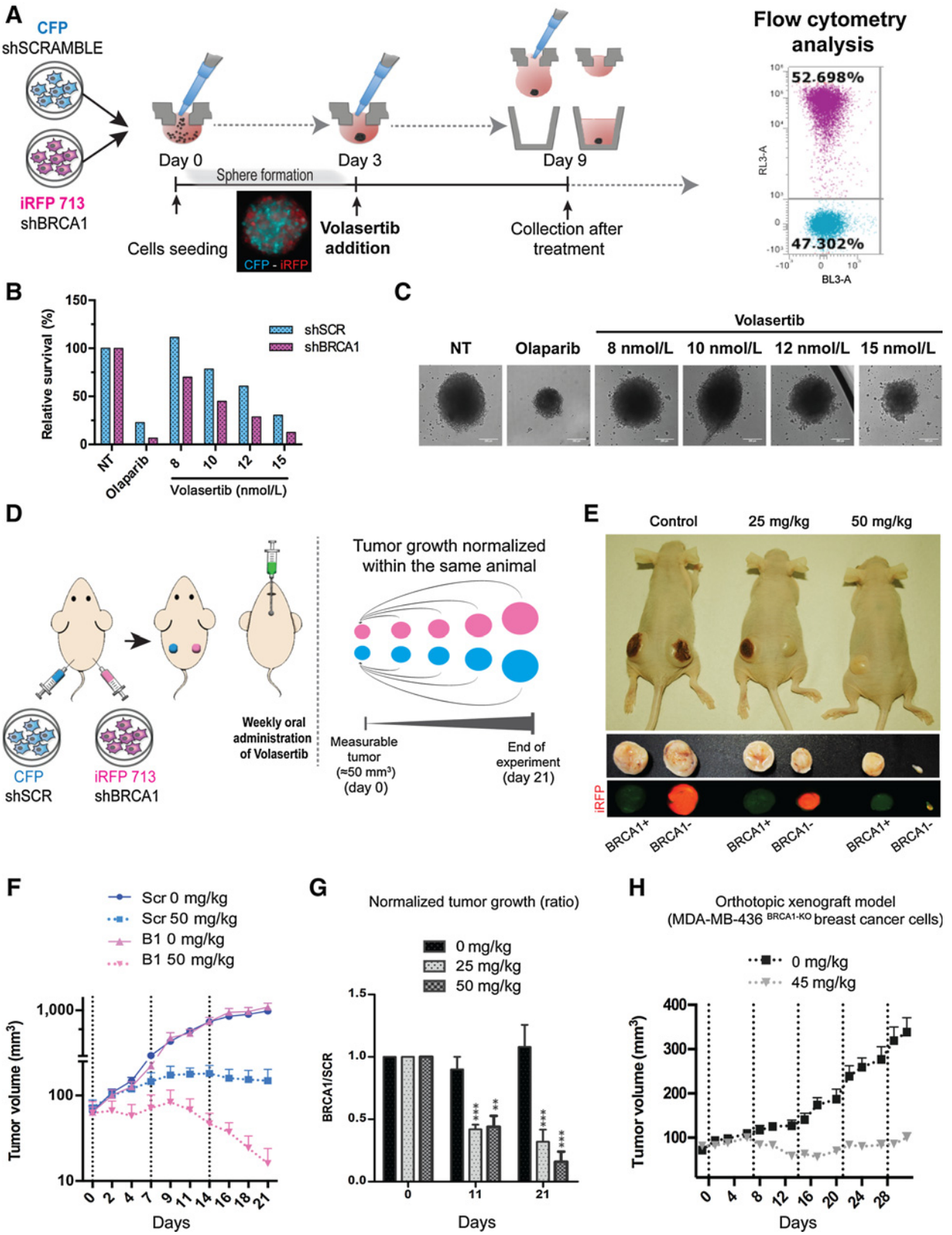

doses of PLK1i in Fig. 2C, F, and H). Given that our goal was to demonstrate *in vivo* that BRCA1 deficiency increases the cellular sensitivity to PLK1 inhibition and triggers SL, we developed an animal model to evaluate such differential sensitivity. Although a possibility would be to compare the sensitivity to PLK1 inhibition using isogenic cell lines in different mice, we hypothesized that the maximum comparability would be reached using single mice as experimental units. Thus, we established a xenograft model where two different types of isogenic cells (BRCA-proficient and BRCA-deficient) were injected to each flank of the same mouse (Fig. 5D). As such, each mouse bears two parallel tumors that only differ in their BRCA1 expression status. This protocol has the advantage that allows the analysis of classical tumor size at given endpoints, but also to estimate the growth curve of each tumor in comparison with the flanking tumor in the same mouse (Fig. 5D, right). We selected an experimental setup where volasertib was administered orally once a week (Supplementary Fig. S5D). We observed that in animals treated with vehicle both BRCA1-proficient and BRCA1-deficient tumors grew at similar rates during the entire length of the experiment (Fig. 5E and F). As reported, volasertib treatment at 50 mg/kg abolished tumor growth of HCT116 cells (shSCR in our experiment) and kept tumors similar to their initial size until the end of the experiment (Fig. 5F; Supplementary Fig. S5E; ref. 41). Strikingly however, BRCA1-deficient tumors were much strongly affected by volasertib, not only inhibiting their growth, but also showing remission to the point of becoming unmeasurable after 3 weeks of treatment (Fig. 5E and F). From a therapeutic point of view, this was an exciting finding because it proved that BRCA1 deficiency alone is enough to trigger increased sensibility to volasertib *in vivo*. Indeed, when we determined the ratio of tumor growth within each mouse, we observed that animals treated with vehicle always presented a ratio near to 1, indicating similar proliferation rates of BRCA1-proficient and BRCA1-deficient tumors. However, animals treated with the optimal reported dose of volasertib (50 mg/kg) presented a ratio of 0.5 at day 11 and 0.25 at the end of the experiment, thus underlining the differential response to the treatment triggered by BRCA1 deficiency (Fig. 5G). Remarkably, we also revealed that decreasing to half the dose of volasertib (25 mg/kg) suffices to induce strong SL in those mice (Fig. 5G; Supplementary Fig. S5F). These findings prompt us to explore a BRCA1-mutant breast cancer mouse model, which more closely resembles the features of the human disease (Supplementary Fig. S5G). We found that, like HCT116^{shBRCA1} cells, MDA-436$^{BRCA1\text{-}KO}$ cells show high sensitivity to volasertib *in vivo* (Fig. 5H; Supplementary Fig. S5G).

High PLK1 expression is observed in low-expressing BRCA1 cells and in patients with triple-negative breast cancer

To study the therapeutic potential of inhibiting PLK1 in BRCA1-deficient patients, we performed a retrospective analysis using The Cancer Genome Atlas database (TCGA; refs. 42–44). Our initial approach was to assess a potential mutual exclusion of BRCA1 and PLK1 tumor mutations in human breast cancers, which would suggest the existence of an SL interaction between these mutations in patients. Although a tendency to coexclusion was observed (Supplementary Fig. S6A), PLK1 mutants were extremely rare (0.2%) and therefore we could only analyze very small patient cohorts. Thus, we decided to study BRCA1 and PLK1 mRNA expression patterns. We observed that while PLK1 and BRCA1 correlate in their expression levels, patients with very low levels of BRCA1 expression were characterized by high levels of PLK1 expression (Fig. 6A, dotted trapezoid). Remarkably, deeper genomic analysis revealed that approximately 75% of low-BRCA1/high-PLK1 patients were basal-like according to the PAM50 subtypes (Fig. 6B) and triple negative for hormone receptors (Supplementary Fig. S6B), in comparison with approximately 18% of each subtype when the complete breast cancer cohort (Supplementary Fig. S6C). To further explore the biological relevance of the high-PLK1 expression observed in patients with low-BRCA1 expression, we went back to the isogenic pairs of cell lines used in the screening and during the validation phase. Our goal was to establish whether the knockdown of BRCA1 alone suffices to trigger an increase in PLK1 expression, and whether the rescue of BRCA1 expression in BRCA1-KO cells is able to revert the overexpression phenotype. Both scenarios were confirmed. Every isogenic cell pair submitted to shRNA^{BRCA1} expression depicted a stable increase in PLK1 levels (Fig. 6C; Supplementary Fig. S6D). A more exacerbated phenotype was observed in the isogenic breast cancer cell pair HCC1937, in which the rescue of BRCA1 expression dramatically reduced PLK1 expression levels (Fig. 6C). Moreover, when we studied markers of PLK1 catalytic activity in these cells, we found that high PLK1 levels correlate with increased pPLK1 and its downstream target pCDK1 (Fig. 6D), thus indicating that these cancer cells present higher levels of PLK1 kinase activity.

Figure 5.

Volasertib triggers selective toxicity in chimeric spheroids and in a two xenograft *in vivo* models. **A,** Protocol used to generate chimeric spheroids. HCT116$^{p21-/-}$ CFP-shSCR and iRFP-shBRCA1 cells were seeded in equal numbers using a 96-well plate with hanging drop technology. Three days later, the assembly of chimeric spheroids was confirmed by microscopy and treatment with volasertib was performed for 6 days. Pools of 10 spheroids per condition were mechanically disaggregated with trypsin and analyzed by flow cytometry. **B,** Dose–response experiment with chimeric spheroids treated with volasertib or olaparib as a positive control. The relative survival of the BRCA1-proficient and -deficient populations calculated in relation to the same populations in the control spheroids is shown. **C,** Representative images of one spheroid per condition before the spheroids' processing by flow cytometry. **D,** Double tumor xenograft model: Human HCT116$^{p21-/-}$ CFP-shSCR or iRFP-shBRCA1 cells were injected in contralateral flanks of individual mice. Once the tumors reached a size of approximately 50 mm^3, volasertib or vehicle was administered orally using a gavage needle. Normalized tumor growth and the normalized ratio are calculated for each animal at different time points. **E,** Representative animals for the control, 25 mg/kg of volasertib, and 50 mg/kg of volasertib groups at the end of the double tumor xenograft experiment. Bottom, the extracted tumors that were also imaged with an infrared scanner to confirm that even the smallest tumors contained the original cells. **F,** Measurements of the tumor volume for the control and 50 mg/kg double tumor groups. Dotted line indicates volasertib administration days. Data represent the mean tumor volume ± SEM ($n = 5$). **G,** Normalized tumor ratio across different time points of the double tumor experiment. Statistical analysis was performed using two-way ANOVA with Bonferroni posttest ($n = 5$; **, $P \leq 0.01$; ***, $P < 0.001$). **H,** Orthotopic xenograft model: Human breast cancer MDA-MD-436$^{BRCA1\text{-}KO}$ cells were injected in mammary fat pad of nude mice. Measurements of tumor volumes for the control and 45 mg/kg volasertib–treated groups are shown. The dotted line indicates volasertib administration days. Data represent the mean tumor volume ± SEM ($n = 13$).

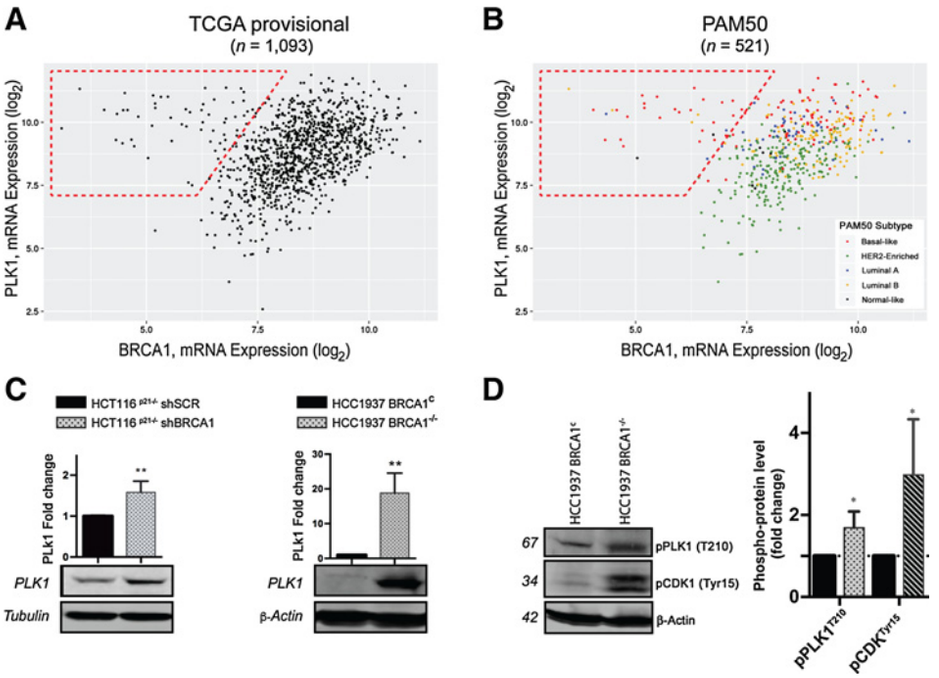

Figure 6.
PLK1 and BRCA1 levels in patients with breast cancer from TCGA and in the isogenic cell lines used in this study. **A,** TCGA analysis showing that tumor samples with low-BRCA1 mRNA expression present high-mRNA expression levels of PLK1 (dotted trapezoid). The complete TCGA provisional database was used for this analysis ($n = 1{,}093$ patients). **B,** A subset of the TCGA database that included information about the PAM50 type of tumors ($n = 521$) was analyzed, and the PAM50 subtypes—basal like, normal like, luminal A, luminal B, and HER2 enriched—were plotted. **C,** Western blot of PLK1 protein levels in isogenic HCT116$^{p21-/-}$ shSCR versus shBRCA1, and BRCA1^{C} versus HCC1937$^{BRCA1\text{-}KO}$ cells. **D,** Western blot showing phospho-PLK1 and phospho-CDK1 levels as markers of catalytic activity of PLK1 in HCC1937$^{BRCA1\text{-}C}$ versus HCC1937$^{BRCA1\text{-}KO}$ cells. Statistical analysis: two-tailed unpaired *t* test (*, $P \leq 0.05$; **, $P \leq 0.01$).

Discussion

An unforeseen SL interaction between PLK1 and BRCA1

Previous reports have explored functional links between PLK1 and BRCA1. Evidence is available in both directions. On the one hand, PLK1 and BRCA1 have been shown to physically interact in cells, being BRCA1 a modulator of PLK1 kinase activity in response to replication stress (45). On the other hand, PLK1 phosphorylates BRCA1 at serine 1164, modulating its double-strand break repair functions (46). Although our results could be, in part, explained by such roles of PLK1 and BRCA1 within the same pathways, the fact that we observe strong SL induction both in BRCA1-deficient and BRCA1-KO models (Fig. 2) suggests that the SL trigger should be associated with compensatory BRCA1 and PLK1 roles that may not be circumscribed to the ones mentioned above. Moreover, our results with BRCA2-deficient cells and with the direct repeats assay (Supplementary Fig. S2) indicate that the observed SL is unlikely linked to the HR deficiency of these cells. Our hypothesis of compensatory pathways is strongly supported by the finding that patients with very low expression levels of BRCA1 display high levels of PLK1 expression (Fig. 6A). In line with this, it was striking to find out that the artificial knockdown of BRCA1 using shRNA sufficed to trigger a stable increase in PLK1 protein levels in the cell lines generated for this study (Fig. 6C; Supplementary Fig. S6D). These results suggest the existence of a universal compensatory response to BRCA1 downregulation and that the SL induction observed in our experiments is linked to an acquired dependence/addiction to PLK1 in BRCA1-deficient cells. But, which might be such a compensatory function of PLK1 and BRCA1? Our data support the notion that the SL phenotype is timely linked to the progression through mitosis. On the one hand, PLK1 has a pivotal contribution to mitosis progression, participating in the mitotic entry, centrosome maturation and duplication cycle, and cytokinesis (28). On the other hand, critical functions for BRCA1 in the progression through mitosis have also been extensively characterized (47, 48). In particular, it has been consistently demonstrated that BRCA1 plays an important role in centrosome duplication, interacting with and promoting the ubiquitination of centrosomal γ-tubulin (29–37). Our studies of centrosomal number and localization led to the identification of giant multinucleated cells with large aggregates of centrosomes (Fig. 3D). Interestingly, we observed that BRCA1-induced deficiency and PLK1 inhibition as single treatments lead to the increase of these aberrant phenotypes above the basal levels. Moreover, the combination of PLK1 inhibition in the dose range that triggers SL induction induces a marked accumulation of these phenotypes in a BRCA1-deficient background (Fig. 3D). Our hypothesis is that such giant multinucleated cells are the consequence of a survival phenotype rather than being a prerequisite for cell death. In fact, SL induction starts to clearly manifest at day 4 (Fig. 2G), while the giant cells are mainly observed at longer end points (Supplementary Fig. S3). Nonetheless, we speculate that these cells are destined to die, presumably by mitotic catastrophe or by cytokinesis failure (49). This assumption is supported by the extremely low clonogenic potential depicted by the surviving population (Fig. 3E). Together, our findings establish a strong synthetic essential link between PLK1 and BRCA1 that unveils a great therapeutic potential of inhibiting PLK1 in this type of malignancies.

A new niche for the therapeutic inhibition of PLK1 in human cancers

A great deal of effort and resources were invested during the past 15 years to move PLK1 inhibitors to the clinic. The FDA has granted the "breakthrough therapy" status to Boehringer's volasertib and the "Orphan Drug" designation to Trovagene's

PCM-075 for the treatment of acute myeloid leukemia. Given to its central role in mitotic coordination, PLK1 inhibition imposes a strong antitumoral effect in many types of cancers, which is highlighted by the numerous ongoing clinical trials. However, the housekeeping roles of PLK1 also implicate undesired adverse effects, which seem to be more extreme in the cardiovascular system (50, 51). Thus, cancers characterized by PLK1 overexpression (13), are likely to respond better to PLK1 inhibitors, triggering attenuated collateral effects. The findings presented in this article unveil a new promising niche to exploit the potential of PLK1 inhibitors. Our unbiased screening approach revealed a dose range where PLK1 inhibitors display almost no cytotoxic effect in $BRCA1^{+}$ cells yet inducing strong SL in BRCA1-deficient cells (Fig. 2). Remarkably, we have also developed chimeric spheroids and an animal model that allowed us to confirm such a differential response to PLK1 inhibition in an *in vitro* 3D context and *in vivo* (Fig. 5). In our SL animal model, BRCA1-deficient tumors reached almost complete remission after only 3 weeks of treatment with oral volasertib, while tumor size remained unchanged in the $BRCA^{+}$ tumors of the same animals (Fig. 5E and F). These thrilling findings point toward the design of clinical trials that consider BRCA1 status as a prognostic maker of therapeutic response to PLK1 inhibitors. Moreover, our retrospective analysis of the TCGA database shows that patients with triple-negative breast cancer (TNBC) present higher expression of PLK1 that non-TNBC (Supplementary Fig. S6B). This finding implies that this type of breast cancers, which are characterized by their limited therapeutic options, could benefit with therapeutic schemes involving PLK1 inhibition, regardless of their BRCA1 status. In addition, our results also position PLK1 as an alternative to PARPi to target BRCA1-deficient cancers. Our evidence indicates that olaparib and volasertib have different mechanisms of action (Figs. 1–4), therefore suggesting that PLK1 inhibitors could become a therapeutic alternative to treat BRCA1-deficient cancers that become resistant to PARPi. In line with this, a recent report proposed the combinatorial use of olaparib and PLK1 inhibitors to treat olaparib-resistant prostate cancer, independently of the BRCA1 status (52). Moreover, the absence of genomic instability induction by volasertib at the SL dose (Fig. 4) suggests that this type of treatment would induce a "clean" type of antitumoral response, attenuating the induction of genomic stability and delaying the acquisition of resistance mechanisms.

Disclosure of Potential Conflicts of Interest

No potential conflicts of interest were disclosed.

Authors' Contributions

Conception and design: S. Carbajosa, K.P. Madauss, V. Gottifredi, G. Soria
Development of methodology: S. Carbajosa, M.F. Pansa, N.S. Paviolo, A.M. Castellaro, A.D. Nigra, I.A. García, L. Rodriguez-Berdini, G.A. Gil, V. Gottifredi, G. Soria
Acquisition of data (provided animals, acquired and managed patients, provided facilities, etc.): S. Carbajosa, A.M. Castellaro, B.L. Caputto, G.A. Gil, J.L. Bocco, V. Gottifredi, G. Soria
Analysis and interpretation of data (e.g., statistical analysis, biostatistics, computational analysis): S. Carbajosa, M.F. Pansa, N.S. Paviolo, A.M. Castellaro, D.L. Andino, A.D. Nigra, A.C. Racca, V. Angiolini, L. Guantay, F. Villafañez, M.B. Federico, M.C. Rodríguez-Baili, K.P. Madauss, I. Gloger, E. Fernandez
Writing, review, and/or revision of the manuscript: S. Carbajosa, M.F. Pansa, A.M. Castellaro, A.D. Nigra, A.C. Racca, I. Gloger, E. Fernandez, V. Gottifredi
Administrative, technical, or material support (i.e., reporting or organizing data, constructing databases): S. Carbajosa, V. Angiolini, I. Gloger
Study supervision: S. Carbajosa, B.L. Caputto, G. Drewes, I. Gloger, E. Fernandez, G.A. Gil, J.L. Bocco, V. Gottifredi, G. Soria
Others (project coordination and administration): G. Soria

Acknowledgments

The authors thank the flow cytometry, microscopy, and cell culture facilities of CIBICI-CONICET for technical support. This work was supported by a consortium grant of FONCyT and the Trust in Science program (Global Health R&D) from GlaxoSmithKline (PAE-GLAXO 2014-0005). Animal work was supported by a Start-Up grant to G. Soria (FONCyT PICT Start-Up 2013-1553). S. Carbajosa and I.A. García are fellows from the PAE-GLAXO 2014-0005. N.S. Paviolo, A.M. Castellaro, A.D. Nigra, A.C. Racca, L. Rodriguez-Berdini, F. Villafañez, M.B. Federico, and M.C. Rodríguez-Baili were supported by fellowships from CONICET. M.F. Pansa was supported by fellowships from the National Institute of Cancer and CONICET. B.L. Caputto, E. Fernandez, G.A. Gil, J.L. Bocco, V. Gottifredi, and G. Soria are researchers from CONICET.

The costs of publication of this article were defrayed in part by the payment of page charges. This article must therefore be hereby marked *advertisement* in accordance with 18 U.S.C. Section 1734 solely to indicate this fact.

Received October 29, 2018; revised February 18, 2019; accepted March 13, 2019; published first March 19, 2019.

References

1. Venkitaraman AR. Cancer suppression by the chromosome custodians, BRCA1 and BRCA2. Science 2014;343:1470–5.
2. Fackenthal JD, Olopade OI. Breast cancer risk associated with BRCA1 and BRCA2 in diverse populations. Nat Rev Cancer 2007;7:937–48.
3. Ramus SJ, Gayther SA. The contribution of BRCA1 and BRCA2 to ovarian cancer. Mol Oncol 2009;3:138–50.
4. Prakash R, Zhang Y, Feng W, Jasin M. Homologous recombination and human health: the roles of BRCA1, BRCA2, and associated proteins. Cold Spring Harb Perspect Biol 2015;7:a016600.
5. Lord CJ, Ashworth A. BRCAness revisited. Nat Rev Cancer 2016;16:110–20.
6. Lord CJ, Ashworth A. PARP inhibitors: synthetic lethality in the clinic. Science 2017;355:1152–58.
7. Kohn EC, Lee JM, Ivy SP. The HRD decision—which PARP inhibitor to use for whom and when. Clin Cancer Res 2017;23:7155–7.
8. D'Andrea AD. Mechanisms of PARP inhibitor sensitivity and resistance. DNA Repair 2018;71:172–6.
9. Mullard A. Synthetic lethality screens point the way to new cancer drug targets. Nat Rev Drug Discov 2017;16:589–91.
10. Quent VMC, Loessner D, Friis T, Reichert JC, Hutmacher DW. Discrepancies between metabolic activity and DNA content as tool to assess cell proliferation in cancer research. J Cell Mol Med 2010;14:1003–13.
11. Hammerstein AF, Wylie PG. Accurate cytotoxicity and proliferation determination: advantages of a high-throughput phenotypic approach over ATP luminescence assays. Assay Drug Dev Technol 2016;14:407–15.
12. Chan GKY, Kleinheinz TL, Peterson D, Moffat JG. A simple high-content cell cycle assay reveals frequent discrepancies between cell number and ATP and MTS proliferation assays. PLoS One 2013;8:e63583.
13. Liu Z, Sun Q, Wang X. PLK1, a potential target for cancer therapy. Transl Oncol 2017;10:22–32.
14. Filonov GS, Piatkevich KD, Ting L-M, Zhang J, Kim K, Verkhusha VV. Bright and stable near-infrared fluorescent protein for *in vivo* imaging. Nat Biotechnol 2011;29:757–61.
15. Trucco LD, Andreoli V, Núñez NG, Maccioni M, Bocco JL. Krüppel-like factor 6 interferes with cellular transformation induced by the H-ras oncogene. FASEB J 2014;28:5262–76.

16. Richardson C, Moynahan ME, Jasin M. Double-strand break repair by interchromosomal recombination: suppression of chromosomal translocations. Genes Dev 1998;12:3831–42.
17. Soria G, Almouzni G. Differential contribution of HP1 proteins to DNA end resection and homology-directed repair. Cell Cycle 2013;12:422–9.
18. Federico MB, Vallerga MB, Radl A, Paviolo NS, Bocco JL, Di Giorgio M, et al. Chromosomal integrity after UV irradiation requires FANCD2-mediated repair of double strand breaks. PLoS Genet 2016;12:e1005792.
19. Mansilla SF, Soria G, Vallerga MB, Habif M, Martínez W, Prives C, et al. UV-triggered p21 degradation facilitates damaged-DNA replication and preserves genomic stability. Nucleic Acids Res 2013;41:6942–51.
20. Joray MB, Villafañez F, González ML, Crespo MI, Laiolo J, Palacios SM, et al. P53 tumor suppressor is required for efficient execution of the death program following treatment with a cytotoxic limonoid obtained from Melia azedarach. Food Chem Toxicol 2017;109:888–97.
21. Janghorban M, Farrell AS, Allen-petersen BL, Pelz C, Daniel CJ, Oddo J, et al. Targeting c-MYC by antagonizing PP2A inhibitors in breast cancer. Proc Natl Acad Sci U S A 2014;111:9157–62.
22. Bunz F. Requirement for p53 and p21 to sustain G2 arrest after DNA damage. Science 1998;282:1497–501.
23. Drewry DH, Wells CI, Andrews DM, Angell R, Al-Ali H, Axtman AD, et al. Progress towards a public chemogenomic set for protein kinases and a call for contributions. PLoS One 2017;12:e0181585.
24. Elkins JM, Fedele V, Szklarz M, Abdul Azeez KR, Salah E, Mikolajczyk J, et al. Comprehensive characterization of the published kinase inhibitor set. Nat Biotechnol 2016;34:95–103.
25. Garuti L, Roberti M, Bottegoni G. Non-ATP competitive protein kinase inhibitors. Curr Med Chem 2010;17:2804–21.
26. Van den Bossche J, Lardon F, Deschoolmeester V, De Pauw I, Vermorken JB, Specenier P, et al. Spotlight on volasertib: preclinical and clinical evaluation of a promising Plk1 inhibitor. Med Res Rev 2016;36:749–86.
27. Kathryn JC, Sireesha V G, Stanley L. Triple negative breast cancer cell lines: one tool in the search for better treatment of triple negative breast cancer. Breast Dis 2012;32:35–48.
28. Petronczki M, Lénárt P, Peters JM. Polo on the rise-from mitotic entry to cytokinesis with Plk1. Dev Cell 2008;14:646–59.
29. Xu X, Weaver Z, Linke SP, Li C, Gotay J, Wang XW, et al. Centrosome amplification and a defective G2-M cell cycle checkpoint induce genetic instability in BRCA1 exon 11 isoform-deficient cells. Mol Cell 1999;3:389–95.
30. Deng CX. Roles of BRCA1 in centrosome duplication. Oncogene 2002;21: 6222–7.
31. Starita LM, Machida Y, Sankaran S, Elias JE, Griffin K, Schlegel BP, et al. BRCA1-dependent ubiquitination of -tubulin regulates centrosome number. Mol Cell Biol 2004;24:8457–66.
32. Sankaran S, Starita LM, Groen AC, Ko MJ, Parvin JD. Centrosomal microtubule nucleation activity is inhibited by BRCA1-dependent ubiquitination. Mol Cell Biol 2005;25:8656–68.
33. Kais Z, Parvin JD. Regulation of centrosomes by the BRCA1-dependent ubiquitin ligase. Cancer Biol Ther 2008;7:1540–3.
34. Kais Z, Chiba N, Ishioka C, Parvin JD. Functional differences among BRCA1 missense mutations in the control of centrosome duplication. Oncogene 2012;31:799–804.
35. Tarapore P, Hanashiro K, Fukasawa K. Analysis of centrosome localization of BRCA1 and its activity in suppressing centrosomal aster formation. Cell Cycle 2012;11:2931–46.
36. Löffler H, Fechter A, Liu FY, Poppelreuther S, Krämer A. DNA damage-induced centrosome amplification occurs via excessive formation of centriolar satellites. Oncogene 2013;32:2963–72.
37. Matsuzawa A, Kanno S ichiro, Nakayama M, Mochiduki H, Wei L, Shimaoka T, et al. The BRCA1/BARD1-interacting protein OLA1 functions in centrosome regulation. Mol Cell 2014;53:101–14
38. Mardin BR, Schiebel E. Breaking the ties that bind: new advances in centrosome biology. J Cell Biol 2012;197:11–8.
39. Murai J, Huang SN, Das BB, Renaud A, Zhang Y, Doroshow JH, et al. Trapping of PARP1 and PARP2 by clinical PARP inhibitors. Cancer Res 2012;72:5588–99.
40. Ito S, Murphy CG, Doubrovina E, Jasin M, Moynahan ME. PARP inhibitors in clinical use induce genomic instability in normal human cells. PLoS One 2016;11:e0159341.
41. Rudolph D, Steegmaier M, Hoffmann M, Grauert M, Baum A, Quant J, et al. BI 6727, A polo-like kinase inhibitor with improved pharmacokinetic profile and broad antitumor activity. Clin Cancer Res 2009;15:3094–102.
42. Cancer Genome Atlas Network. Comprehensive molecular portraits of human breast tumours. Nature 2012;490:61–70.
43. Gao J, Aksoy BA, Dogrusoz U, Dresdner G, Gross B, Sumer SO, et al. Integrative analysis of complex cancer genomics and clinical profiles using the cBioPortal. Sci Signal 2013;6:pl1.
44. Cerami E, Gao J, Dogrusoz U, Gross BE, Sumer SO, Aksoy BA, et al. The cBio Cancer Genomics Portal: an open platform for exploring multidimensional cancer genomics data. Cancer Discov 2012;2:401–4.
45. Zou J, Rezvani K, Wang H, Lee KS, Zhang D. BRCA1 downregulates the kinase activity of Polo-like kinase 1 in response to replication stress. Cell Cycle 2013;12:2255–65.
46. Chabalier-Taste C, Brichese L, Racca C, Canitrot Y, Calsou P, Larminat F, et al. Polo-like kinase 1 mediates BRCA1 phosphorylation and recruitment at DNA double-strand breaks. Oncotarget 2016;7:2269–83.
47. Starita LM, Parvin JD. The multiple nuclear functions of BRCA1: transcription, ubiquitination and DNA repair. Curr Opin Cell Biol 2003;15:345–50.
48. Venkitaraman AR. Linking the cellular functions of *BRCA* genes to cancer pathogenesis and treatment. Annu Rev Pathol Mech Dis 2009; 4:461–87.
49. Vakifahmetoglu H, Olsson M, Zhivotovsky B. Death through a tragedy: mitotic catastrophe. Cell Death Differ 2008;15:1153–62.
50. Raab M, Kappel S, Krämer A, Sanhaji M, Matthess Y, Kurunci-Csacsko E, et al. Toxicity modelling of Plk1-targeted therapies in genetically engineered mice and cultured primary mammalian cells. Nat Commun 2011;2: 395.
51. De Cárcer G, Wachowicz P, Martínez-Martínez S, Oller J, Méndez-Barbero N, Escobar B, et al. Plk1 regulates contraction of postmitotic smooth muscle cells and is required for vascular homeostasis. Nat Med 2017; 23:964–74.
52. Li J, Wang R, Kong Y, Broman MM, Carlock C, Chen L, et al. Targeting Plk1 to enhance efficacy of olaparib in castration-resistant prostate cancer. Mol Cancer Ther 2017;16:469–79.